Effect of Input Resistance Voltage-Dependency on DC Estimate of Membrane Capacitance in Cardiac Myocytes

M. Zaniboni,* F. Cacciani,* and M. Groppi†
*Dipartimento di Biologia Evolutiva e Funzionale-Sezione Fisiologia, and †Dipartimento di Matematica, Università degli Studi di Parma, Parma, Italy

ABSTRACT The measure of membrane capacitance (C_m) in cardiac myocytes is of primary importance as an index of their size in physiological and pathological conditions, and for the understanding of their excitability. Although a plethora of very accurate methods has been developed to access C_m value in single cells, cardiac electrophysiologists still use, in the majority of laboratories, classical direct current techniques as they have been established in the early days of cardiac cellular electrophysiology. These techniques are based on the assumption that cardiac membrane resistance (R_m) is constant, or changes negligibly, in a narrow potential range around resting potential. Using patch-clamp whole-cell recordings, both in current-clamp and voltage-clamp conditions, and numerical simulations, we document here the voltage-dependency of R_m, up to −45% of its resting value for 10-mV hyperpolarization, in resting rat ventricular myocytes. We show how this dependency makes classical protocols to misestimate C_m in a voltage-dependent manner (up to 20% errors), which can dramatically affect C_m-based calculations on cell size and on intracellular ion dynamics. We develop a simple mechanistic model to fit experimental data and obtain voltage-independent estimates of C_m, and we show that accurate estimates can also be extrapolated from the classical approach.

INTRODUCTION

The value of membrane capacitance (C_m) is a measure of how much charge is needed to displace cell polarization, how fast cell membrane passively responds to current/voltage changes, and how large is the membrane surface area. C_m and input resistance (R_m) of excitable cells are usually referred to as passive electrical properties and derived referring to an equivalent circuit, parallel combination of the two electrical elements. Microelectrode and patch-clamp techniques which have been developed, under current-clamp (CC) and voltage-clamp (VC) conditions, to solve this parallel RC combination to calculate C_m (1,2), can be grouped in two categories: the alternating current (AC) and the direct current (DC) methods. Very accurate estimates of C_m are achieved using AC methods, by means of single or multiple sinusoidal command voltages, used to clamp the cell with two-phase lock-in amplifiers (3,4). Square-wave stimulations are also employed and analyzed in the frequency domain (5), and ramp command voltage protocols have been recently improved (6) and applied to cardiac myocytes (7,8). These techniques have been originally established and largely employed mainly to study changes in membrane area during exocytosis and endocytosis (3,9,10), but they are still too technically demanding for a more general use (6) like the estimate of cell size in cardiac preparations.

The measure of specific C_m ($\mu F/cm^2$) in cardiac tissue and, since the introduction of enzymatic isolation procedures, of C_m (pF) in single cardiac myocytes, has been pursued from the early days of cardiac electrophysiology (11–13), given the pivotal role of this parameter in cardiac excitability and the physiopathological interest in monitoring cell size in the heart. Systematic errors in the measure of C_m will lead, for example, to erroneous evaluation of cardiomyocytes remodeling in studies where this parameter is measured in hypertrophied hearts (7,14,15), failing hearts (16), dilated cardiomyopathy (17), diabetes (18), and myocardial infarction (19). Such errors will also affect studies on intercellular electrotonic interactions (20–22) where C_m plays a primary role in determining source-sink properties of interacting cells. Finally, they will affect those studies where C_m is measured to normalize transsarcolemmal ion currents and fluxes through carriers to cell surface and, indirectly, to cell volume (23).

Definitely the more common tool adopted by cardiac electrophysiologists to measure C_m remains the use of time-domain DC methods, where constant current (or voltage) steps are imposed to the cell membrane and the study of the resulting voltage (or current) displacements is performed in terms of mono-exponential functions (1), a procedure which, as recently pointed out (6), has not been modified substantially since its introduction 30 years ago (24). This approach is based on the assumption that C_m is constant for a given cell, and that R_m is fairly constant over membrane potential (V_m) changes (1), at least in the voltage range of application of the mentioned protocols. Since R_m changes have been documented around the resting potential (V_r) (cited below), the second assumption is actually that these changes are negligible with respect to C_m estimate.

The fact that R_m changes during the cardiac action potential follows directly from the Hodgkin-Huxley theory of membrane excitability, has been described by Weidmann in early days (25), and recently measured in guinea pig ventricular myocytes (22). In addition, Weidmann, by means

Submitted March 15, 2005, and accepted for publication June 22, 2005.

Address reprint requests to M. Zaniboni, Tel.: 05-21-905623; E-mail: zaniboni@biol.unipr.it.

0006-3495/05/09/2170/12 $2.00

doi: 10.1529/biophysj.105.062828

of constant current injections into cardiac fibers, noticed that R_m continuously decreased, starting from threshold V_m toward rest and for increasingly hyperpolarizing current injections. The decrease of R_m as membrane potential hyperpolarizes with respect to threshold potential, is accounted for in cardiac myocytes mainly by inward rectification of I_{K1} (26,27) and has already been measured in isolated rat ventricular myocytes (13,28).

In the present work, we show that R_m voltage-changes around V_r are indeed not negligible when standard CC/VC protocols are used to calculate C_m, which therefore results to be voltage-dependent as well. To this end, we measure the $R_m(V_m)$ function around V_r and incorporate it in a mechanistic RC equivalent model, which better resembles membrane passive electrical properties. The numerical solution of such circuit allows accurate estimates of C_m which do not depend on voltage. We suggest that I_{K1} rectification, as the main responsible for the input resistance voltage dependency, is also the primary source for the error in C_m estimate through the classical approach. This study, performed in turn, on real isolated rat ventricular myocytes, on five different mathematical models of the cardiac action potential, and on a simple RC mathematical model, also suggests a simplified procedure that allows to derive accurate estimates of C_m with the classical constant CC and VC protocols.

MATERIALS AND METHODS

Cell isolation

Single cells were obtained by enzymatic dispersion of adult (6 months, 400–500 g) male Wistar rat left ventricles. After thoracotomy, the heart was rapidly removed, mounted on a Langendorff apparatus, and perfused at 37°C with the following sequence of solutions: Ca^{2+}-free (control, no added calcium) Tyrode solution for 5 min to remove the blood, low-Ca^{2+} (0.1 mM) solution containing 1 mg/ml type 2 collagenase (Worthington, Lakewood, NJ) and 0.1 mg/ml type XIV protease (Sigma Aldrich, Milan, Italy) for 20 min, and enzyme-free low- Ca^{2+} solution for 5 min. The left ventricle was then minced and shaken for 10 min in the low-Ca^{2+} solution. Myocytes were stored at room temperature in the control solution with 0.5 mM Ca^{2+}. All experiments were performed within 2–8 h after isolation. All myocytes used in this study had well-defined striations and did not spontaneously contract.

Solutions

Isolation solution contained 126 mM NaCl, 22 mM dextrose, 5.0 mM $MgCl_2$, 4.4 mM KCl, 20 mM taurine, 5 mM creatine, 5 mM Na pyruvate, 1 mM NaH_2PO4, and 24 mM HEPES (pH = 7.4 adjusted with NaOH). The solution was gassed with 100% O_2. Control solution for cell bathing during experiments contained 126 mM NaCl, 11 mM dextrose, 5.4 mM KCl, 1.0 mM $MgCl_2$, 1.08 mM $CaCl_2$, and 24 mM HEPES (pH-adjusted to 7.4 with NaOH). The pipette filling solution contained 113 mM KCl, 10 mM NaCl, 5.5 mM dextrose, 5 mM K_2ATP, 0.5 mM $MgCl_2$, and 10 mM HEPES (pH-adjusted to 7.1 with KOH). A drop of cells was placed in the experimental chamber (~2.5 ml) and superfused by gravity at a flow rate of ~2 ml/min. The temperature of the solutions in the cell bath was 37°C.

Electrical recordings

Suction pipettes were made from borosilicate capillary tubing (Harvard Apparatus, Edenbridge, United Kingdom) and had a resistance, when filled, of 2–4 MΩ. Transmembrane potential and current (i) were recorded by means of an Axoclamp 2B amplifier (Axon Instruments, Union City, CA) adopting the whole-cell configuration of the patch-clamp technique.

Classical DC protocols to measure C_m

Here we summarize time-domain DC methods for the estimate of C_m which have been adopted and criticized in this study. For the sake of clarity, we will consider the resting membrane potential V_r set to zero.

CC approach

Cells were held in whole-cell configuration (amplifier in Bridge mode) and injected at a frequency of 2 Hz, with 200-ms constant current pulses (i_p) usually starting from −0.260 nA and incrementing with 5-pA steps up to 0.235 nA. Subthreshold voltage deflections were sampled at 5 kHz, digitized (Digidata 1200 Series Interface, Axon Instruments, Union City, CA), and best fitted with mono-exponential functions (Kaleidagraph, Synergy Software, Reading, PA) as solutions

$$V_m(t) = i_p \times R_m \times (1 - e^{-t/\tau}); \quad V_m(0) = V_r = 0; \quad \tau = R_m \times C_m \tag{1}$$

of the equation

$$\dot{V}_m(t) = \frac{1}{C_m} \times \left(i_p - \frac{V_m(t)}{R_m} \right), \tag{2}$$

relative to the linear equivalent parallel RC circuit. It is straightforward to derive the plateau value of $V_m(t)$ as $V_\infty = i_p \times R_m$. The description does not include any additional series pipette resistance R_s, which was electrically compensated with bridge balance. Passive electrical properties R_m and C_m were derived as best-fitting parameters of experimental voltage traces with Eq. 1.

VC approach, curve fit

To minimize filtering effects due to pipette capacitance, pipettes tips were coated with a hydrophobic compound (Sylgard, Dow Corning, Midland, MI) and the cell bath was maintained at a low level (1 mm). Protocol features were analogous to current clamp; with the amplifier in discontinuous single-electrode voltage-clamp mode, cells were initially clamped at their V_r and then stepped with 40-ms constant voltage-clamps (V_c) usually starting from V_r − 20 mV and incrementing with 1-mV steps up to V_r + 15 mV. Current traces were best fitted with mono-exponentials as linear functions

$$i(t) = (V_c - V_m(t))/R_s \tag{3}$$

of the solutions

$$V_m(t) = \frac{R_p}{R_s} \times V_c \times (1 - e^{-t/(R_p \times C_m)});$$
$$V_m(0) = V_r = 0; \quad R_p = \frac{R_s \times R_m}{R_s + R_m} \tag{4}$$

of the equation

$$\dot{V}_m(t) = \frac{1}{C_m} \times \left(\frac{V_c - V_m(t)}{R_s} - \frac{V_m(t)}{R_m} \right), \tag{5}$$

relative to the linear equivalent parallel RC circuit in series with an additional access resistance R_s. R_m, C_m, and R_s were derived as best fitting parameters. Membrane potential V_∞, corresponding to the plateau value of the current ($i_\infty = V_c / (R_m + R_s)$), was derived as $V_c - i_\infty \times R_s$, being the additional R_s uncompensated during the protocol.

In the following discussion, we will use the notation $\Delta V_m = V_\infty - V_r = V_\infty$ for the steady-state value reached by V_m during CC and VC protocols.

VC approach, area of the transient

An alternative VC method to measure C_m, to which we refer in this work, is to measure the charge under the current transient and divide it by the $\Delta V = V_c - V_r$. This is often approximated as

$$C_m = \frac{Q}{\Delta V}, \quad (6)$$

where Q is the area under the current transient and above i_∞. Recently a better approximation for this is adopted (16) as

$$C_m = \frac{Q + i_\infty \times \tau}{\Delta V}, \quad (7)$$

where Q is the area under the current transient and above i_∞ and $i_\infty \times \tau$ is an approximation for the area under i_∞ and above the exponential resistive component of the current response.

Computer simulations

The electrical properties of single resting cardiomyocytes were simulated, in turn, using membrane equations from the mathematical models listed in Table 1, or solving Eq. 2 and Eq. 5 for a simple RC circuit including a series resistance R_s, which was set to zero in CC simulations. Equations were numerically solved using an adaptive Euler method for the LR91 model, and a fifth-order Runge-Kutta method for PD01 model and for the RC circuit. Simulations on the LR94, PB01, and RM00 were performed on the Cell Electrophysiology Simulation Environment (CESE Version 1.3.4, available on http://cese.sourceforge.net). All simulations were performed on a Pentium IV processor and codes for LR91, PD01, and for the RC circuit implemented in MatLab language (The MathWorks, Natick, MA).

Statistics

Results are presented as mean ± SE. Statistical analysis was performed using the unpaired Student's *t*-test with SPSS software (SPSS, Chicago, IL). Statistical significance was set at $P < 0.05$.

RESULTS

Estimate of an input resistance voltage-function

The membrane input resistance (R_m) of single rat ventricular myocytes was measured within $\sim\pm10$ mV around resting potential (V_r) through CC and VC protocols (see Materials and Methods). Fig. 1 *A* shows voltage deflections from a CC protocol and the function $R_m(\Delta V_m)$ well fitted by a parabola $c_0 + c_1 \times \Delta V_m + c_2 \times \Delta V_m^2$ with $c_0 = 58.35$, $c_1 = 3.64$, and $c_2 = 0.14$. The same analysis performed on 12 myocytes gave an average parabolic fitting of $c_0 = 55.99 \pm 3.67$, $c_1 = 2.37 \pm 0.25$, and $c_2 = 0.06 \pm 0.01$. Current traces from a VC protocol are reported in Fig. 1 *B* with the function $R_m(\Delta V_m)$, which is similar to the one measured in CC, and well fitted by a parabola with $c_0 = 54.22$, $c_1 = 4.51$, and $c_2 = 0.12$. The same analysis performed on 12 myocytes gave an average fitting of $c_0 = 58.76 \pm 6.95$, $c_1 = 5.22 \pm 0.59$, and $c_2 = 0.15 \pm 0.02$. When the two protocols were numerically simulated on a LR91 model, they returned a qualitatively analogous function $R_m(\Delta V_m)$, well fitted by a parabola with $c_0 = 21.71$, $c_1 = 1.10$, and $c_2 = 0.027$. Similar $R_m(\Delta V_m)$ behavior was found in all five mathematical models employed (see below).

TABLE 1 The different mathematical models tested in their subthreshold electrical properties

Cell type	Reference	Abbreviation
Mammalian ventricular	Luo and Rudy (42)	LR91
Guinea pig ventricular	Luo and Rudy (43)	LR94
Rabbit ventricular	Puglisi and Bers (44)	PB01
Rat ventricular	Pandit et al. (30)	PD01
Canine atrial	Ramirez et al. (45)	RM00

Estimate of the capacitance for a non-Ohmic RC

A constant R_m around resting potential V_r (which we will refer to as the Ohmic assumption in the following discussion) is required in classical DC measurements of C_m. If, as shown above, R_m changes up to 30–50 MΩ within ±10 mV around V_r, the solution of a non-Ohmic circuit that includes the $R_m(\Delta V_m)$ function (which we will call the non-Ohmic assumption) should be more appropriate.

In Fig. 2 we show examples in which C_m was calculated (see Materials and Methods) by mono-exponential fittings of the voltage/current traces reported in Fig. 1. The measured C_m varies with ΔV_m, decreasing with membrane polarization. The same analysis performed on seven myocytes led to C_m changes, as measured from a linear fitting for $-10\text{ mV} < \Delta V_m < 0$ mV, of 2.95 ± 0.74 pF/mV in CC and 1.35 ± 0.54 pF/mV in VC. Analogous results are shown, for example, on the more general LR91 model. Analyzing a non-Ohmic RC as if it was Ohmic clearly leads to an error in C_m estimate, which increases with the displacement of membrane potential from V_r, doing more so in CC than in VC. The CC protocol was applied also on the other mathematical models listed in Table 1, and results reported in Fig. 3. In the lower panel of the same figure, the relationship between the relative error in C_m estimate and R_m rectification is also reported for the five mathematical models and for the experimental data. To better isolate this effect, we solved two simple mathematical models of a resting myocyte in whole-cell configuration, which included only R_s, C_m, and R_m (Fig. 4). R_m was kept constant in a first case (Fig. 4 *A*) and voltage-dependent in a second case (Fig. 4 *B*). Fig. 4 *A* shows the symmetrical behavior (with respect to the resting potential/current) of voltage and current traces obtained when the Ohmic circuit (Fig. 4 *A*) was solved, in turn, in CC and VC conditions. When the constant R_m of the circuit was replaced (as in Fig. 4 *B*) with an experimental $R_m(\Delta V_m)$ function of the type shown in Fig. 1, the voltage and current deflections lost their symmetry and appeared more like those measured in real cells. Traces were all analyzed in terms of mono-exponential fittings (see Materials and Methods), assuming each time, for R_m, the constant value measured at plateau,

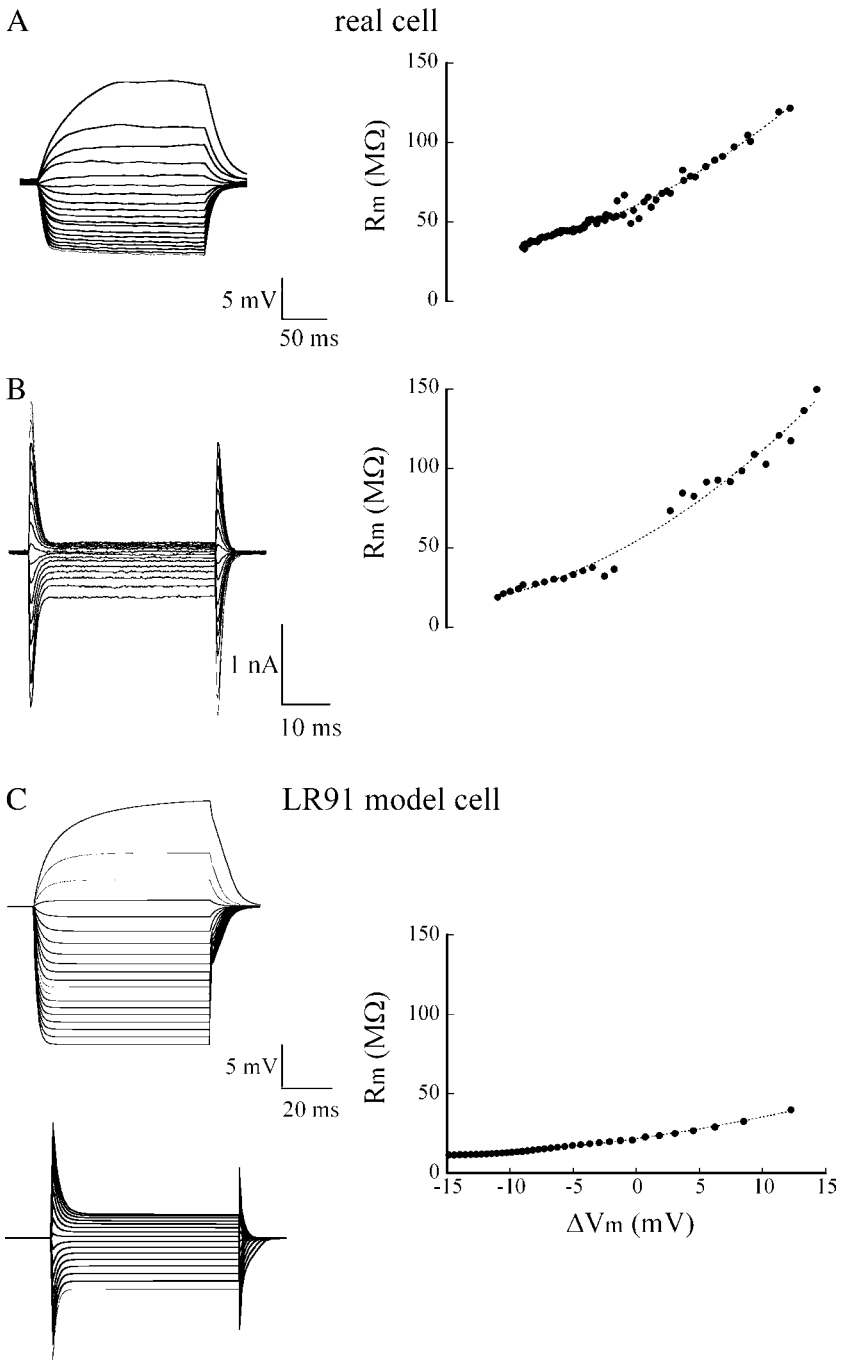

FIGURE 1 Measure of R_m voltage-dependency. Left column: (*A*) voltage deflections from a CC protocol on a rat myocyte. Only one in every four traces is shown for clarity. (*B*) Current traces from a VC protocol on a different myocyte. Only one in every second trace is shown. (*C*) Analogous CC and VC protocols simulated on the LR91 model ($R_s = 5$ MΩ in VC). Right column: R_m, calculated from plateau values of each voltage and current trace, is reported (*solid circles*) as a function of ΔV_m, fitted by parabolic functions (*dotted lines*).

and C_m values derived and reported as solid circles in Fig. 4 *C*. The Ohmic assumption, in the case of a physiologically non-Ohmic RC circuit, leads to an error in the estimate of C_m which qualitatively reproduces what we found in real myocytes and in the mathematical model cells (Fig. 2 and Fig. 3), with C_m varying with a sigmoidal-law around the resting potential.

In Fig. 5 two additional examples of C_m derived through mono-exponential fittings in two real ventricular myocytes are shown. In addition, the $R_m(\Delta V_m)$ parabolic functions, derived from both cells, were, in turn, included in a mathematical non-Ohmic model equivalent to the one in Fig. 4 *B*. The value R_s was also derived from the VC protocols, and was included in the model. Each voltage and current trace was then fitted with numerical solutions of the non-Ohmic form of Eq. 2 and Eq. 5 including the experimentally derived $R_m(\Delta V_m)$, to obtain new estimates of C_m (see Appendix for details on the algorithm), also reported in the figures. Whereas C_m, measured in the Ohmic assumption, is voltage-dependent and varies ~2.1 pF/mV in CC and 1.9 pF/mV in VC, the values derived upon considering the non-Ohmic assumption were fairly constant within the voltage range

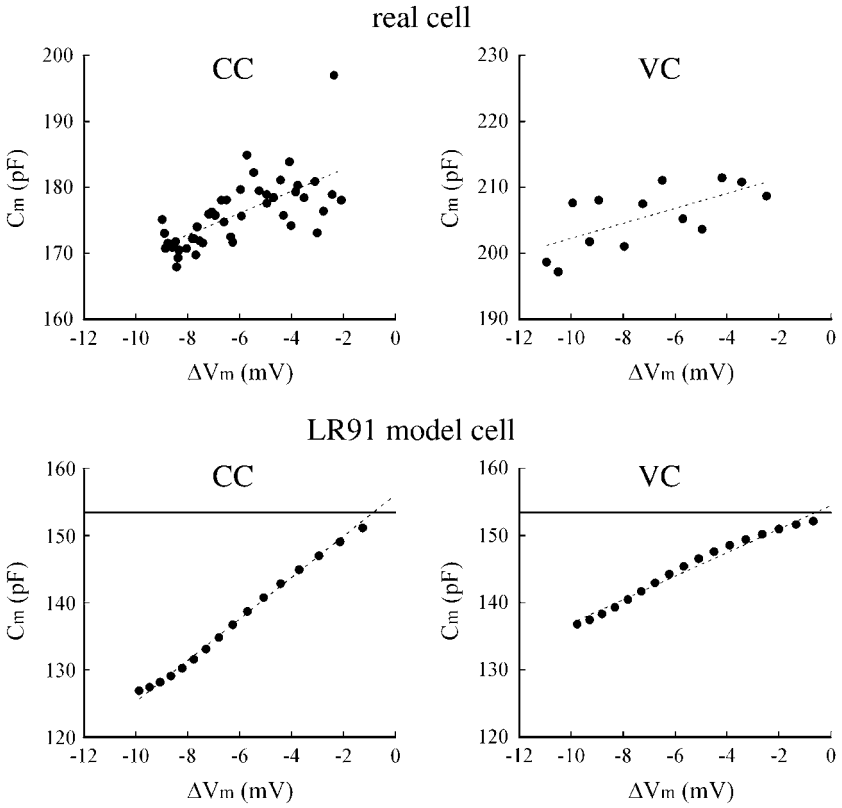

FIGURE 2 Estimated C_m as a function of V_m displacement from V_r. (*Top*) Each solid circle represents a DC estimate of C_m from experimental traces of Fig. 1, *A* and *B*. (*Bottom*) Same for the traces from the LR91 model in Fig. 1 *C*, where C_m was set to 153.44 pF (*horizontal lines*) on the basis of the geometrical considerations of Luo and Rudy (43). Dotted lines in each panel represent linear fittings of the experimental data, 1.6, 1.1, 3.1, and 1.7 pF/mV, respectively.

under study, being 128.4 ± 0.6 pF in CC and 150.2 ± 1.1 pF in VC. Same result (voltage-independent estimates of C_m) was obtained when all five mathematical model cells were studied within the non-Ohmic assumption (not shown). For an additional control, we numerically simulated the CC and VC real experiment on two non-Ohmic model circuits like the one in Fig. 4 *B*, including, respectively, the non-Ohmically calculated two mean values of the C_m, the $R_m(\Delta V_m)$ functions and R_s. When we fitted the numerically integrated voltage and current traces with mono-exponentials, we found a continuous $C_m(\Delta V_m)$ function that well fits the C_m values Ohmically derived from experimental data. The same type of analysis was performed with analogous results on seven current-clamped and seven voltage-clamped ventricular myocytes where C_m values from different cells were normalized for comparison to the constant value found each time with non-Ohmic assumption, which was set to 1. Average error in normalized C_m estimate was 0.0189 mV^{-1} in CC and 0.0097 mV^{-1} in VC. Analogous results were obtained when C_m was measured in the LR91 model (Fig. 6). In summary, when, instead of using mono-exponential fittings, we solved a mechanistic model including the R_m (ΔV_m) derived from the simulated traces, we were able to measure, at least in a 10–15-mV range below V_r, a value of C_m that tightly resembles the actual one.

Another way, used in early works, to study the time course of voltage deflections in constant step-CC experiments, was to plot the logarithm of the voltage displacement as a function of time (13,1), which should result in a straight line in the case of mono-exponential rise. In Fig. 7 *A* we show, in a real cell, the time course of a voltage displacement from a CC protocol, together with the time course of its logarithm, respectively fitted with a mono-exponential and a straight line (C_m derived as 152 pF). Although other traces from the same experiment revealed a 10-MΩ difference between R_m measured at $V_\infty = -8$ mV and $V_\infty = -4$ mV (Fig. 7, *arrows*), which in turn resulted in a 20-pF difference in the C_m estimate at the two potentials, both fittings showed a very high ($R = 0.999$) correlation with experimental curves. A good mono-exponential fitting correlation or a quasi-linear relation between $\ln(\Delta V_m)$ and time do not guarantee, along with the associated experimental noise, the Ohmicity of the tested RC and thus the independency of R_m from V_m. When the same voltage deflection was analyzed with the least-squares algorithm (see Appendix) based on the non-Ohmic circuit (Fig. 7 *B*), the best-fitting solution corresponded to a $C_m = 193$ pF, which changed very little (mean ± SE = 0.7) in all the analyzed traces from $V_\infty = -1$ to $V_\infty = -10$ mV.

Effect of C_m size on the error in the estimate of C_m using the Ohmic assumption

The assumption of a constant R_m for the cell membrane leads to errors in the estimate of C_m as shown above. To investigate whether this error, described in Fig. 4 as a sigmoidal $C_m(\Delta V_m)$ function centered at the resting potential, depends

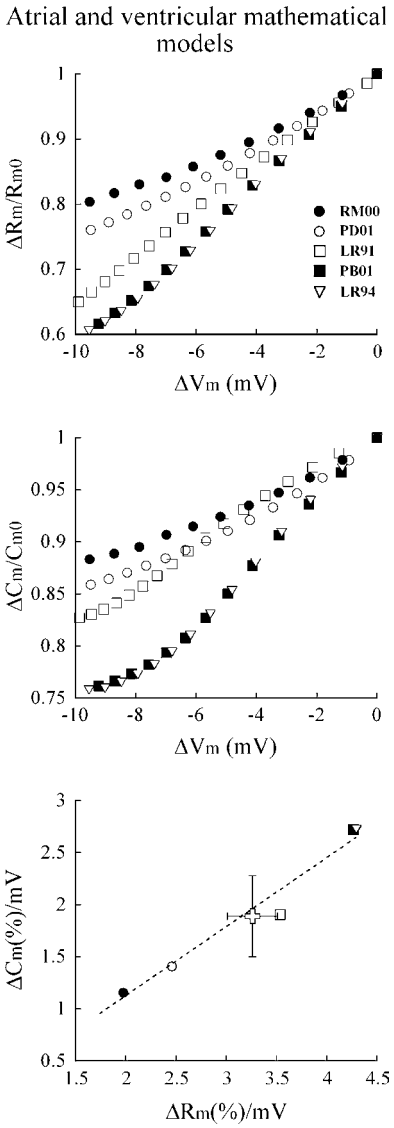

FIGURE 3 Voltage-dependency of R_m and of the estimated C_m in five mathematical models of cardiomyocytes. (*Top*) $R_m(\Delta V_m)$ as obtained through the CC protocol applied to the five mathematical models listed in Table 1. (*Middle*) $C_m(\Delta V_m)$ obtained with the same protocol. Results were normalized to the extrapolated resting values of R_m (R_{m0}) and C_m (C_{m0}), which were respectively set to *1* for comparison. (*Bottom*) The above traces were linearly fitted within the −10/0 mV ΔV_m range, to plot the slope of $C_m(\Delta V_m)$ versus the slope of $R_m(\Delta V_m)$ for the five models. The cross symbol represents the corresponding averaged estimate made on seven current-clamped rat ventricular myocytes ($1.89 \pm 0.39\ mV^{-1}$ vs. $3.26 \pm 0.25\ mV^{-1}$), also cited in the Results.

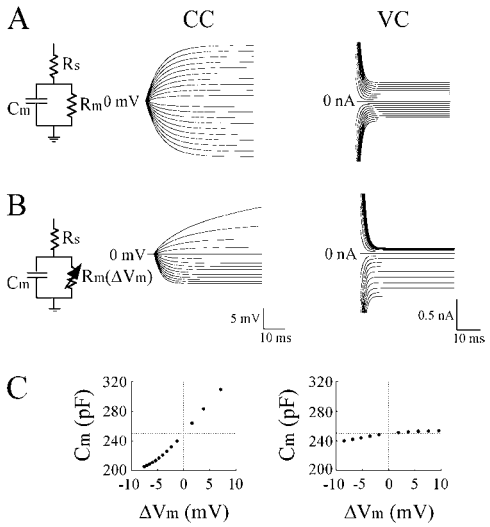

FIGURE 4 DC estimate of C_m in Ohmic and non-Ohmic RC circuits. (*A*) Current-clamped (from −0.25 to 0.25 nA, step 0.025 nA) voltage displacements and voltage-clamped (from −20 to +20 mV, step 2 mV) current traces, mathematically simulated on the circuit reported on the left, with $R_m = 56.5\ M\Omega$ and $C_m = 250$ pF. R_s was set to 0 MΩ in CC and 5 MΩ in VC. (*B*) Identical protocols simulated on the same circuit were $R_m(\Delta V_m) = 56.5 + 4.8 \times \Delta V_m + 0.17 \times \Delta V_m^2\ M\Omega$. (*C*) C_m versus ΔV_m, as calculated from mono-exponential fittings of the traces in *B* (*solid circles*).

on the actual C_m value of the cell, we performed simulations on a simple RC model including an experimentally derived parabolic $R_m(\Delta V_m)$, and, in turn, three different values for C_m. Simulated traces were fitted with mono-exponentials in the Ohmic assumption and measured $C_m(\Delta V_m)$ functions were reported as solid lines in Fig. 8, *A* and *B*. A typical non-Ohmic $R_m(\Delta V_m)$ function, like the one used here, led to a −11.8% (CC) and −2.4% (VC) errors in the estimate of C_m at $\Delta V_m = -10$ mV in a 265 pF cell. When cell capacitance was increased by 50%, this error decreased to −10.5% in CC and did not change in VC, whereas a 50% decrease of C_m led to an increase of error up to −12.7% in CC and again no changes in VC. We then repeated the test for a series of C_m from 5 to 1000 pF. Interestingly, we found that, as the cell capacitance increased, the error in C_m estimate monotonically decreased from an initial value of 13.3% in CC, whereas it remained fairly constant at 2.8% in VC (with $R_s = 5$ MΩ). When R_s was increased to 20 MΩ, the error increased in VC up to 5.6% for a $C_m = 5$ pF, and monotonically decreased to 4.2% for a $C_m = 1000$ pF. To summarize, the percentage error in C_m estimate decreases with the increasing of C_m, being less important in voltage than in current clamp. The error in VC-estimate of C_m depends on the uncompensated series resistance R_s.

Effect of the slope of $R_m(\Delta V_m)$ function on the error in the estimate of C_m using the Ohmic assumption

We performed additional simulations to investigate how the slope of the $R_m(\Delta V_m)$ function affects the error in C_m estimate. We chose three different $R_m(\Delta V_m)$ parabolic functions (Fig. 8 *D*) differing in the first-order coefficient (~±50% from a central value of 1.5) and all ranging within measured experimental values. We then run CC and VC simulations for an RC circuit including, in turn, the three $R_m(\Delta V_m)$ functions and having a $C_m = 265$ pF (Fig. 8, *E* and *F*). With the increasing of the slope of the $R_m(\Delta V_m)$ function,

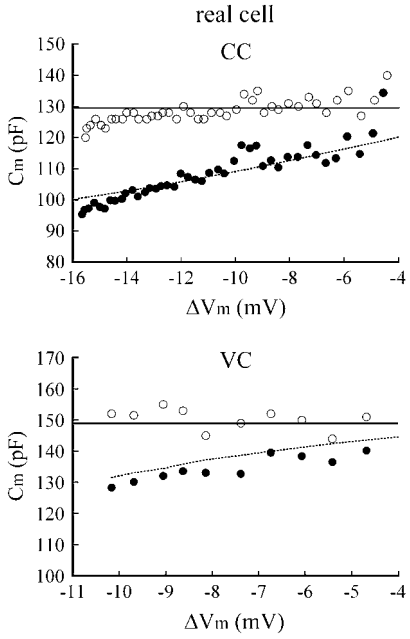

FIGURE 5 Comparison of C_m estimate with Ohmic and non-Ohmic assumption in real ventricular myocytes. C_m, first calculated through mono-exponential fittings of CC-elicited voltage traces (*top*), and VC-elicited current traces (*bottom*), plotted as a function of ΔV_m (*solid circles*). C_m is also reported as derived through the algorithm which assumes non-Ohmicity of the circuit (*open circles*). Solid line represents the average value of C_m in the non-Ohmic assumption. This value, together with calculated R_s and $R_m(\Delta V_m)$, is incorporated in an equivalent circuit whose solutions, in CC and VC simulations, are fitted with mono-exponentials to derive C_m for each ΔV_m (*dotted lines*).

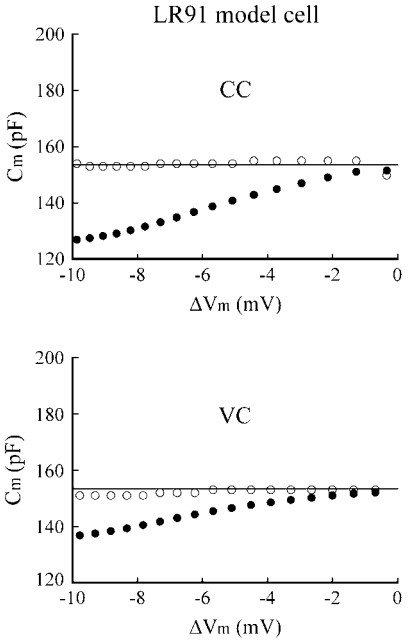

FIGURE 6 Comparison of C_m estimate with Ohmic and non-Ohmic assumption in the LR91 model cell. C_m, as calculated adopting the Ohmic assumption (*solid circles*) and the non-Ohmic assumption (*open circles*) through a CC and a VC protocol on the LR91 model. Horizontal lines represent the actual C_m of the model. A series resistance of 10 MΩ was added in VC simulations.

the error in the estimate of C_m, as measured at $\Delta V_m = -10$ mV, increased both in CC and VC from values of 4.4% and 0.7%, respectively (lower slope function) up to 22.4% and 7.5% (higher slope function).

Good enough estimates of C_m with the Ohmic assumption

From the simulations performed on the non-Ohmic RC model in Fig. 4, it appears that the sigmoidal function of the estimated $C_m(\Delta V_m)$, derived assuming a constant R_m, has the property that it crosses the horizontal line corresponding to the actual value of C_m in the resting membrane potential ($\Delta V_m = 0$). Moreover the slope of this function is fairly constant in the V_m range of interest (-10 mV $< \Delta V_m <$ 0 mV), where it can be approximated with a straight line. It follows that the proper value of cell capacitance could be, in principle, extrapolated with only two current injections (or VC pulses) experiments, using mono-exponential fittings, and ignoring therefore the voltage-dependency of R_m. Histograms in Fig. 9 show, for both CC and VC, average estimates of C_m, taken ignoring R_m voltage-dependency and adopting mono-exponential fittings (*first* and *second columns* in each panel), deriving R_m voltage-dependency and using the least-squares fitting procedure (*third column*), or assuming the function $C_m(\Delta V_m)$ to be linear and extrapolating the zero-potential value from two measures, taken approximately at $\Delta V_m = -10$ mV and $\Delta V_m = -5$ mV, for each cell (*fourth column*). The average value obtained with the extrapolation procedure does not significantly differ in CC and VC from the one measured with the non-Ohmic assumption.

DISCUSSION

Among the several ways developed to measure C_m, we focus the present study on the time-domain analysis of square-wave stimulations (as defined in Ref. 2) and the limitations we found in applying this technique to measure C_m in single rat ventricular myocytes. The use, adopted within this approach, of the mono-exponential solutions 1 and 3 of Eq. 2 and Eq. 5 in a subthreshold V_m range, coincides with the assumption that R_m is constant in this range or, at least, its changes do not appreciably affect C_m calculation. We show here that R_m voltage-dependency around V_r makes C_m estimates, through the classical exponential fittings, also voltage-dependent, and that such dependency can be removed by using a mechanistic RC model that includes R_m changes. As an alternative, a better estimate of C_m can be extrapolated from at least two Ohmic measurements on the same cell. The finding of a voltage-dependency also when C_m was measured in a very general model of the ventricular action potential like LR91, as well as in other more complex

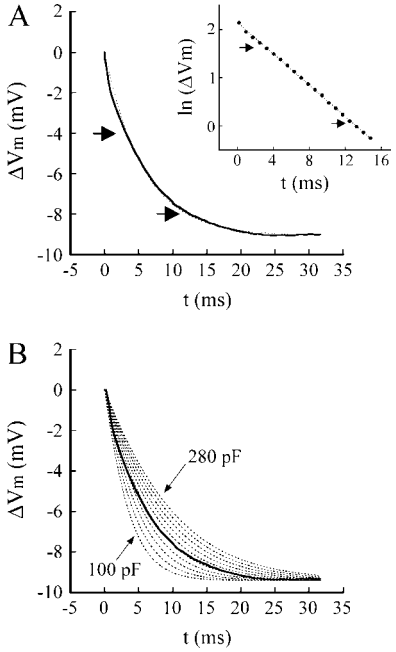

FIGURE 7 Ohmic and non-Ohmic analysis of a current-clamped voltage deflection. (*A*) Mono-exponential fitting (*dotted line*) ($\tau = 5.7$ ms) of a current-clamped (−0.24 nA) voltage displacement (*solid line*) from a ventricular myocyte. (*Inset*) Linear fitting (*dotted line*) of the logarithm of ΔV_m (*solid circles*; only one in every four experimental samples is plotted). (*B*) Dotted lines are solutions of Eq. 2 with $R_m(\Delta V_m) = 9.7 + 2.7 \times \Delta V_m + 0.06 \times \Delta V_m^2\, M\Omega$, experimentally derived from the same cell, and for C_m values from 100 pF to 280 pF (only 1 in every 20 solutions is reported); solid line is the experimental voltage deflection.

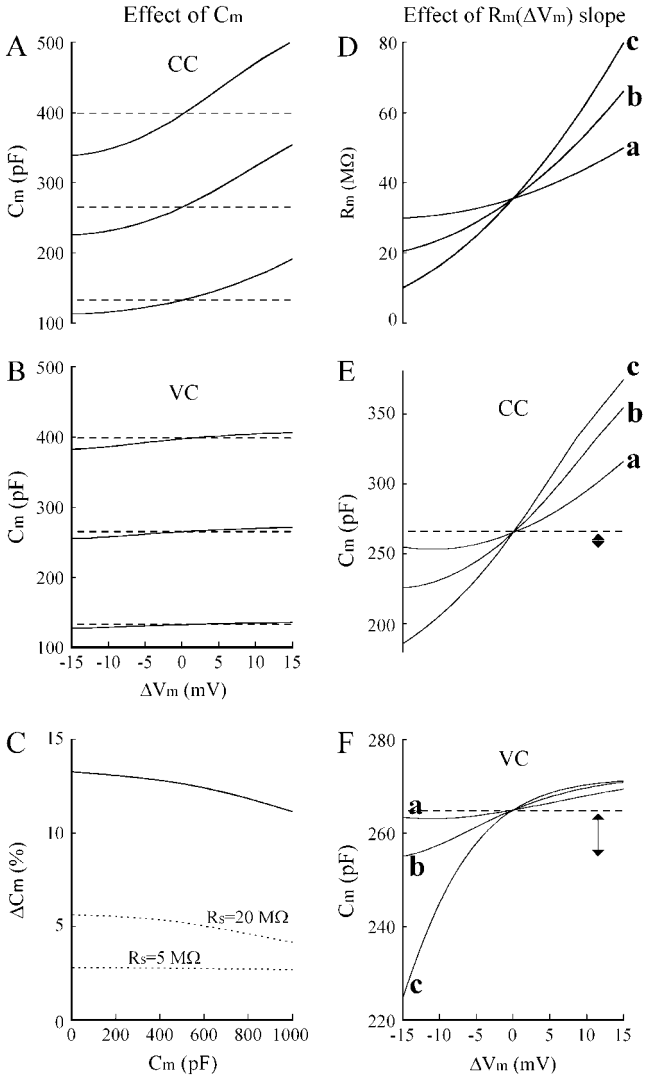

FIGURE 8 Effect of C_m and $R_m(\Delta V_m)$-slope on the accuracy of C_m estimate in a simple RC circuit. (*A* and *B*) CC and VC estimate of C_m through Ohmic assumption on an RC model including an $R_m(\Delta V_m) = 35.5 + 1.5 \times \Delta V_m + 0.034 \times \Delta V_m^2\, M\Omega$ and an $R_s = 5$ MΩ (in VC), for three different values of C_m (*horizontal dotted lines*). (*C*) Error in C_m estimate (percent underestimate from the actual C_m), as measured at $\Delta V_m = -10$ mV, for different values of C_m, in CC (*solid line*) and VC (*dotted lines*) simulated tests, and for two values of R_s. (*D*) Three $R_m(\Delta V_m)$ parabolic functions differing for the slope. (*E* and *F*) CC and VC estimates of C_m by Ohmic assumption on an RC model including, in turn, the three functions. The double-arrow symbols represent the typical experimental noise level in C_m estimate.

mathematical models, rules out the possibility that such effect could be, even only partially, due to experimental artifacts like time- or voltage-changes in R_s or changes in experimental parameters other than those (R_m, C_m, R_s) included in the simple representation of Fig. 4 *B*.

It should be noted that a frequently adopted variant of constant step VC protocol to measure C_m is the one (see Materials and Methods) based on the calculation of the charge underlying the capacitive current transient. An earlier version of this approach simply calculated C_m as in Eq. 6. Such calculation is not accurate and has been more recently replaced by Eq. 7, where the mono-exponentially derived time constant τ appears explicitly, and therefore makes this protocol suffer as well from the voltage-dependency of R_m. Indeed, errors in C_m calculations using Eq. 7 have been derived for the voltage-clamp simulation reported in Fig. 4 *B* without finding any difference from those derived with the classical protocol (data omitted for the sake of clarity). Therefore we did not discuss in a separate section errors in C_m estimate derived with the numerical integration of the current transient during voltage steps.

Limits of the Ohmic assumption

R_m voltage-dependency for subthreshold potentials is known in cardiac tissue at a cellular level (13,27), and has a part in explaining subthreshold behavior of extracellular membrane polarization (29). We limited the majority of our experimental work and analysis on R_m changes in the ~10 mV hyperpolarized V_m-range of well polarized ($V_r = -73.45 \pm 0.69$ mV) rat left-ventricular cells ($n = 24$). With this, we deliberately wanted to avoid eliciting the time-dependent processes that develop in cardiac membrane for depolarizing potentials (e.g., activation of inward sodium current, inward L-type calcium current, calcium-independent transient outward

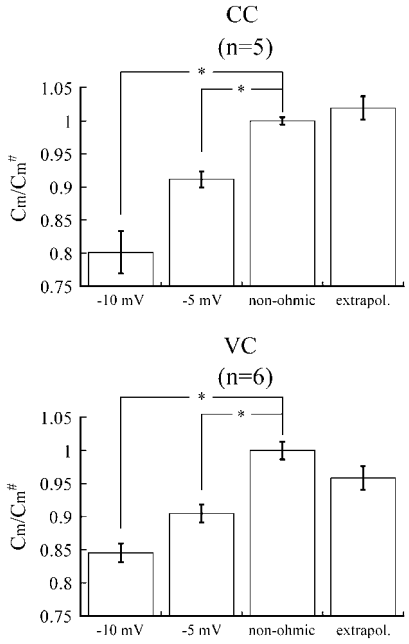

FIGURE 9 Histograms comparing CC and VC estimate of C_m with Ohmic and non-Ohmic assumption in real ventricular myocytes. (*First* and *second bars*) Estimate made through the Ohmic assumption at $\Delta V_m = -10$ mV and $\Delta V_m = -5$ mV, respectively. (*Third bar*) Estimate made through the non-Ohmic assumption ($C_m^{\#}$). (*Fourth bar*) Estimate made through extrapolation from pairs of Ohmic-assumption measurements. All bars are normalized to third bar, which is set to *1* (the asterisk symbol indicates significant differences).

potassium current, steady-state outward potassium current; Ref. 30) and for more hyperpolarized potentials (e.g., I_{K1} time-dependent block and I_f activation; Ref. 31). In fact, voltage traces always reached a plateau within CC steps, as well as current traces never showed time-dependent components other than the capacitive peak during VC steps on tested ventricular myocytes.

The 40–50% decrease of R_m when membrane potential was current- or voltage-clamped from V_r to (V_r-10) mV (see Fig. 1) is reflected into the progressive compression/broadening of the elicited voltage/current traces. In the case of the mathematical LR91 model, the 40% decrease of R_m for $\Delta V_m = -10$ mV, corresponds to a 72% increment of g_{K1} whereas other ionic conductances included in the model do not change (carried simulations not shown). Indeed, this is also the case for the other more complex mathematical models, where, in this subthreshold region, the *I-V* relationship with the highest degree of nonlinearity is that of I_{K1} which, moreover, overwhelms all the others in absolute intensity. In fact, the simple analysis of published steady-state I_{K1}-*V* curves recorded in rat and other mammals ventricular myocytes (e.g., Refs. 32–35) shows that I_{K1} starts rectifying at potentials that are at least 10- or 15-mV hyperpolarized, with respect to the typical V_r for this cell type, which has to be reflected in some R_m voltage-dependency. From our simulation work, we can rule out the direct contribution to R_m rectification of the electrogenic sodium-potassium pump, whose *I-V* relationship is linear in the subthreshold region of interest of this study (see, for example, I_{NaK} equations in PD01, LR94, RM00, and Ref. 36). For the same reason, we can exclude calcium, sodium, and potassium background currents which, although flowing in this voltage range, are usually formulated as linear leakage currents therefore not possibly contributing directly to any R_m rectification (see, for example, related equations in PD01 and LR94). It is tempting to hypothesize a significant role of the sodium-calcium exchanger current, whose IV relationship slightly deviates from linearity in the same region (30,37), but this would need further mathematical and experimental work to be confirmed and quantified. Furthermore, it is possible that some other rectifying mechanisms would be present that are still not included in the models and, therefore, in our knowledge of membrane electrical properties.

A major point of the present work is to show that the measure of C_m within the Ohmic assumption is voltage-dependent in a non-negligible manner. Indeed such dependency was always present in tested ventricular myocytes (Figs. 2 and 5), being less dramatic in VC than in CC, and only slightly depending on the actual value of C_m (see experiment in Fig. 8). In this regard, it is interesting to note the 26-pF difference, reported by Tseng and co-authors in canine ventricular myocytes, between average C_m estimates when measurements were performed in CC (voltage displacements up to -10 mV) and VC (-5 or -10 mV steps) by microelectrode impalement (38). According to our findings, both values underestimate the actual C_m, being the CC error at 54 pF worst than the VC error at 80 pF.

A voltage-dependency in the estimate of C_m can actually become hard to detect and therefore negligible, for example, in hyperkalemic conditions where I_{K1}-*V* curve shifts horizontally toward depolarized potentials and vertically toward more positive currents, becoming therefore more linear around its reversal potential (see $[K^+]_o$-dependency of I_{K1} equation in Ref. 33, and in Ref. 30). The same $[K^+]_o$-dependency can be viewed in the total steady-state *I-V* relationship (e.g., Ref. 38). When $[K^+]_o$ increases, the slope of $R_m(\Delta V_m)$ function becomes smaller and errors in the estimate of C_m will be negligible compared with experimental noise. If we consider, for example, the experiment in Fig. 8 *D*, a cardiac myocyte with an $R_m(\Delta V_m)$ function *a*, characterized by a very weak voltage-dependency, will bring about, when analyzed in VC through the Ohmic assumption (Fig. 8 *F*), an underestimate of C_m, as measured at $\Delta V_m = -10$ mV, $<1\%$, which will be masked within the typical noise level ($\sim$5–6%) of our experiments. On the other hand, an increase in series resistance, especially in cells with higher $R_m(\Delta V_m)$ slope, can produce appreciable differences also in VC, whereas in CC, differences are always measurable practically in all physiological conditions. This is noteworthy, particularly if we consider that, although the great majority of recent cardiac cellular electrophysiological studies

adopts VC constant pulses to measure C_m (e.g., Refs. 39 and 40), many still use the CC approach (21,22), which will then lead to much larger errors.

C_m measurements within homogeneous cell populations suffer frequently for a consistent dispersion (SD often up to 50% of the average) which could be attenuated with the non-Ohmic assumption, allowing better resolution of C_m changes following different pathological conditions or pharmacological treatments. Moreover, errors in C_m evaluation can complicate calculations on intracellular ion dynamics. For example a 10% underestimate of C_m (pF) leads to an 11% overestimate of current density (pA/pF), a 4% underestimate of cell volume in rat ventricular cardiomyocyte (23), and therefore an analogous overestimate of intracellular ion concentration changes. Cell volume and intracellular ion concentration changes will be further underestimated (up to 10%) in species like rabbit, where volume/surface relation is steeper (23).

The correlation, found in the four ventricular models and the one atrial model analyzed, between the slope of the relative error in C_m estimate and the slope of $R_m(\Delta V_m)$ (Fig. 3, *bottom panel*), furthermore emphasizes the generality of the principle: the input resistance of resting cardiomyocytes rectifies in the subthreshold voltage range under study, and such rectification brings about a proportional error in C_m estimate. This proportionality is fully satisfied by our experimental data, as shown by their position on the correlation line of Fig. 3 (*bottom panel*). Interesting to note is the failure of the PD01 model to exactly reproduce rat data in this correlation plot, most likely due to the particular I_{K1} equation chosen in the original work (30), where, on the other hand, the authors themselves recognize the nonuniform properties of I_{K1} across the ventricle as one of the potential limitations of their mathematical description (see also Ref. 41).

A mechanistic non-Ohmic assumption

We call the model described in Fig. 4 *B* ''mechanistic'' because it is based only on properties of an experimental observable (R_m), independently on its biological determinants (ion channels, pumps, exchangers, etc.). This simple model shows that the property of R_m to vary parabolically with V_m is enough, by itself, to qualitatively explain voltage and current asymmetry in response to symmetric current-/voltage-clamp protocols. It also accounts for the voltage-dependency of C_m estimate in vivo and in the mathematical model cells. Finally it shows that, even though mono-exponential functions fit quite well the solutions of Eq. 2 and Eq. 5 for the non-Ohmic circuit, nevertheless they are solutions of a wrong model of the cell electrical properties and they lead therefore to wrong C_m estimates. If, instead, numerical solutions of Eq. 2 and Eq. 5 including the $R_m(\Delta V_m)$ relation are used, the C_m measure becomes independent from V_m and gives estimates that are only a little dispersed around a mean value (Fig. 5), as can also be appreciated in the cell model simulations (e.g., Fig. 6). A further validation of the consistency of the least-square algorithm (see Appendix) to measure C_m comes from the experiment in Fig. 5. A mechanistic mathematical model of a real rat ventricular myocyte, built with experimentally derived $R_m(\Delta V_m)$, R_s, and a constant C_m calculated with the least-square protocol on the same cell, was challenged with CC and VC constant steps and analyzed in terms of mono-exponentials. The fact that the resulting C_m values fit well those derived with the Ohmic assumption on the real cell, demonstrates that the voltage-dependency of R_m is enough to explain the error in C_m estimate, and no other effects like leaky seals, additional uncompensated stray capacitances, series resistances, or different equivalent circuits (11), in principle, need to be considered.

It could be argued that the least-square algorithm presented in this study as a tool to calculate C_m in a voltage-independent manner is too complicated and demanding, especially for what concerns off-line numerical processing of the data, making it therefore not suitable for the general purpose of monitoring passive electrical properties, which is often ancillary in most cardiac cellular electrophysiological studies. To answer this concern, we propose a procedure where an algebraic property of the C_m calculation with the Ohmic assumption is used to extrapolate the real value of C_m without need of any further experimental or mathematical work, as summarized in Fig. 9. Some authors use protocols where symmetrical (depolarizing and hyperpolarizing) VC steps are imposed to the membrane and C_m averaged from the analysis of the two opposite current transients (e.g., Ref. 15). It should be noted that this procedure is quite different from the one we are suggesting here and can also lead to misestimate of C_m, because C_m error in the Ohmic assumption is not symmetrical with respect to V_r (see curve *c* in Fig. 8 *F*).

Why VC gives a better C_m estimate

The typical first-order linear differential equation generating mono-exponential functions as solutions is of the type

$$\dot{y}(t) = a - b \times y(t), \tag{8}$$

where a and b are constants. This is, for example, the form of Eq. 2 of CC in the Ohmic case when R_m is constant. Conversely, when R_m becomes a function of V_m, Eq. 2 assumes a qualitatively different form, whose solutions will always deviate from mono-exponentials as much as R_m is voltage-dependent.

In the case of Eq. 5 of VC, this can be conveniently rewritten as

$$\dot{V}_m(t) = \frac{V_c}{C_m \times R_s} - \frac{V_m(t)}{C_m \times R_s}\left(1 + \frac{R_s}{R_m(V_m)}\right), \tag{9}$$

where it becomes evident that the linear form of Eq. 8 tends to be restored when $R_m \gg R_s$.

This explains qualitatively why, assuming the same voltage-dependency of R_m, VC-derived current traces deviate less from mono-exponentials than CC-derived voltage displacements. In other words, provided R_s is kept much lower than R_m, VC gives best estimates of C_m, as we demonstrated in this study with both experimental and numerical approaches.

Limitations of the study

A limitation of this work is that, although the very general mechanism of subthreshold R_m rectification is presented with its implications on C_m estimate, the relative role of the ionic mechanisms underlying this property have not been unambiguously defined in vivo nor in silico. Although, as in previous studies (26,27), a primary contribution of I_{K1} is strongly suggested, additional experimental and numerical work will help to better define the possible role of sodium-calcium exchanger or other ionic mechanisms in R_m rectification. Also, we do not report here on any intervention made to modify the different ionic mechanisms of R_m voltage-dependency. Work in this direction will be required, for example, to investigate whether there are conditions where the membrane of resting cardiomyocytes behaves Ohmically, helping to better explain its subthreshold electrical properties in physiological and pathological states.

CONCLUSIONS

This study emphasizes that attention should be paid to the subthreshold voltage-dependency of R_m if C_m is to be measured with classical DC protocols. Large errors always arise from the CC approach, but VC can also be substantially affected. Accurate measures can be achieved by taking R_m (ΔV_m) into account in the analysis of CC and VC experimental results or by ignoring this voltage-dependency, and extrapolating results obtained from at least two different ΔV_m values to $\Delta V_m = 0$.

It is straightforward to hypothesize that the voltage-dependency of R_m would also play a role in other techniques to measure C_m, especially those based on complex impedance analysis, widely adopted in the literature and based on the AC study of the same Eq. 2 and Eq. 5.

APPENDIX

The non-Ohmic form of Eq. 2 and Eq. 5 includes an R_m which is not a constant, but is, instead, a function of the membrane potential. Whatever this function (we used second-order polynomials from experimental fittings in this work), it is not possible to find explicitly the solutions for these new equations, which we should solve numerically.

Fitting procedure with the non-Ohmic solutions

Current-clamp

A set of traces like those in Fig. 1 *A* was fitted with mono-exponentials to derive the parabolic functions $R_m(\Delta V_m)$ and $C_m(\Delta V_m)$. $R_m(\Delta V_m)$ was replaced into Eq. 2, which was then solved numerically for each current i_p, for all the C_m values of an n-long vector $\hat{C}_m = [C_{m,1}, C_{m,2}, C_{m,3}, \ldots, C_{m,n}]$, where $C_{m,n}$ and $C_{m,1}$ were, respectively, the central value of the derived C_m range $\pm$ 50 pF. In the case of the experiment shown in Fig. 5, for example, the non-Ohmic form of Eq. 2 was solved for 42 i_p values and, for each i_p, 100 times for C_m values from 65 to 165 pF. For each current injection, the sum of the squared-errors between the numerically integrated solutions and the experimental vector was calculated n times to obtain an n-long vector LS. The actual C_m was then derived as the element of $\hat{C}_m$ that minimizes LS (least-squares method). An example of this procedure is reported in Fig. 7 *B*.

Voltage-clamp

Same approach as in current-clamp, where Eq. 5 was solved for a given set of voltage steps V_c and, for each voltage-clamped V_c, for all the elements of the vector $\hat{C}_m$.

The authors thank Emilio Macchi and Ken Spitzer for helpful comments and suggestions on the article.

This study was supported by grants from the Italian Ministry of Education, University, and Research (grant No. MIUR-COFIN 2003), and the San Paolo di Torino Foundation.

REFERENCES

1. Kado, R. T. 1993. Membrane area and electrical capacitance. *Methods Enzymol.* 221:273–299.
2. Gillis, K. D. 1995. Techniques for membrane capacitance measurements. *In* Single-Channel Recording, 2nd Ed. B. Sakmann and E. Neher, editors. Plenum Press, New York and London. 155–197.
3. Lindau, M., and E. Neher. 1988. Patch-clamp techniques for time-resolved capacitance measurements in single cells. *Pflugers Arch.* 411:137–146.
4. Santos-Sacchi, J. 2004. Determination of cell capacitance using the exact empirical solution of partial differential Y/partial differential C_m and its phase. *Biophys. J.* 87:714–727.
5. Thompson, R. E., M. Lindau, and W. W. Webb. 2001. Robust, high-resolution, whole cell patch-clamp capacitance measurements using square wave stimulation. *Biophys. J.* 81:937–948.
6. Schmitt, B. M., and H. Koepsell. 2002. An improved method for real-time monitoring of membrane capacitance in *Xenopus laevis* oocytes. *Biophys. J.* 82:1345–1357.
7. Ryder, K. O., S. M. Bryant, and G. Hart. 1993. Membrane current changes in left ventricular myocytes isolated from guinea pigs after abdominal aortic coarctation. *Cardiovasc. Res.* 27:1278–1287.
8. Li, Y., Z. Y. Lu, J. M. Xiao, J. Ma, H. Y. Niu, N. Liu, and Y. F. Ruan. 2003. Effect of imidapril on heterogeneity of slow component of delayed rectifying K^+ current in rabbit left ventricular hypertrophic myocytes. *Acta Pharmacol. Sin.* 24:681–686.
9. Johnson, S. L., M. V. Thomas, and C. J. Kros. 2002. Membrane capacitance measurement using patch clamp with integrated self-balancing lock-in amplifier. *Pflugers Arch.* 443:653–663.
10. Debus, K., and M. Lindau. 2000. Resolution of patch capacitance recordings and of fusion pore conductances in small vesicles. *Biophys. J.* 78:2983–2997.
11. Fozzard, H. A. 1966. Membrane capacity of the cardiac Purkinje fibre. *J. Physiol.* 182:255–267.
12. Weidmann, S. 1970. Electrical constants of trabecular muscle from mammalian heart. *J. Physiol.* 210:1041–1054.
13. Powell, T., D. A. Terrar, and V. W. Twist. 1980. Electrical properties of individual cells isolated from adult rat ventricular myocardium. *J. Physiol.* 302:131–153.
14. Stilli, D., A. Sgoifo, E. Macchi, M. Zaniboni, S. De Iasio, E. Cerbai, A. Mugelli, C. Lagrasta, G. Olivetti, and E. Musso. 2001. Myocardial

remodeling and arrhythmogenesis in moderate cardiac hypertrophy in rats. *Am. J. Physiol. Heart Circ. Physiol.* 280:H142–H150.

15. Cerbai, E., M. Barbieri, Q. Li, and A. Mugelli. 1994. Ionic basis of action potential prolongation of hypertrophied cardiac myocytes isolated from hypertensive rats of different ages. *Cardiovasc. Res.* 28:1180–1187.
16. Terracciano, C. M., S. E. Harding, D. Adamson, M. Koban, P. Tansley, E. J. Birks, P. J. Barton, and M. H. Yacoub. 2003. Changes in sarcolemmal Ca entry and sarcoplasmic reticulum Ca content in ventricular myocytes from patients with end-stage heart failure following myocardial recovery after combined pharmacological and ventricular assist device therapy. *Heart J.* 24:1329–1339.
17. Thuringer, D., E. Deroubaix, A. Coulombe, E. Coraboeuf, and J. J. Mercadier. 1996. Ionic basis of the action potential prolongation in ventricular myocytes from Syrian hamsters with dilated cardiomyopathy. *Cardiovasc. Res.* 31:747–757.
18. Arikawa, M., N. Takahashi, T. Kira, M. Hara, T. Saikawa, and T. Sakata. 2002. Enhanced inhibition of L-type calcium currents by troglitazone in streptozotocin-induced diabetic rat cardiac ventricular myocytes. *Br. J. Pharmacol.* 136:803–810.
19. Pinto, J. M., F. Yuan, B. J. Wasserlauf, A. L. Bassett, and R. J. Myerburg. 1997. Regional gradation of L-type calcium currents in the feline heart with a healed myocardial infarct. *J. Cardiovasc. Electrophysiol.* 8:548–560.
20. Spitzer, K. W., N. Sato, H. Tanaka, L. Firek, M. Zaniboni, and W. R. Giles. 1997. Electrotonic modulation of electrical activity in rabbit atrioventricular node myocytes. *Am. J. Physiol.* 273:H767–H776.
21. Huelsing, D. J., K. W. Spitzer, J. M. Cordeiro, and A. E. Pollard. 1998. Conduction between isolated rabbit Purkinje and ventricular myocytes coupled by a variable resistance. *Am. J. Physiol.* 274:H1163–H1173.
22. Zaniboni, M., A. E. Pollard, L. Yang, and K. W. Spitzer. 2000. Beat-to-beat repolarization variability in ventricular myocytes and its suppression by electrical coupling. *Am. J. Physiol. Heart Circ. Physiol.* 278:H677–H687.
23. Satoh, H., L. M. Delbridge, L. A. Blatter, and D. M. Bers. 1996. Surface/volume relationship in cardiac myocytes studied with confocal microscopy and membrane capacitance measurements: species-dependence and developmental effects. *Biophys. J.* 70:1494–1504.
24. Adrian, R. H., and W. Almers. 1974. Membrane capacity measurements on frog skeletal muscle in media of low ion content. *J. Physiol.* 237:573–605.
25. Weidmann, S. 1951. Effect of current flow on the membrane potential of cardiac muscle. *J. Physiol.* 115:227–236.
26. Noble, D. 1975. The Initiation of the Heartbeat. Clarendon Press, Oxford, UK.
27. Schanne, O. F., M. Lefloch, B. Fermini, and E. Ruiz-Petrich. 1990. Membrane resistance increases when automaticity develops in explanted rat heart cells. *Am. J. Physiol.* 258:H145–H152.
28. Zaniboni, M., A. Rossini, F. Cacciani, and E. Musso. 2004. Spontaneous electrical uncoupling in double-current clamped cardiac myocyte pairs. *Biophys. J.* 86:295a (Abstr.).
29. Sambelashvili, A. T., V. P. Nikolski, and I. R. Efimov. 2003. Nonlinear effects in subthreshold virtual electrode polarization. *Am. J. Physiol. Heart Circ. Physiol.* 284:H2368–H2374.
30. Pandit, S. V., R. B. Clark, W. R. Giles, and S. S. Demir. 2001. A mathematical model of action potential heterogeneity in adult rat left ventricular myocytes. *Biophys. J.* 81:3029–3051.
31. Ranjan, R., N. Chiamvimonvat, N. V. Thakor, G. F. Tomaselli, and E. Marban. 1998. Mechanism of anode break stimulation in the heart. *Biophys. J.* 74:1850–1863.
32. Clark, R. B., R. A. Bouchard, E. Salinas-Stefanon, J. Sanchez-Chapula, and W. R. Giles. 1993. Heterogeneity of action potential waveforms and potassium currents in rat ventricle. *Cardiovasc. Res.* 27:1795–1799.
33. Cordeiro, J. M., K. W. Spitzer, and W. R. Giles. 1998. Repolarizing K^+ currents in rabbit heart Purkinje cells. *J. Physiol.* 508:811–823.
34. Rozanski, G. J., Z. Xu, K. Zhang, and K. P. Patel. 1998. Altered K^+ current of ventricular myocytes in rats with chronic myocardial infarction. *Am. J. Physiol.* 274:H259–H265.
35. Xu, Z., and G. J. Rozanski. 1998. K^+ current inhibition by amphiphilic fatty acid metabolites in rat ventricular myocytes. *Am. J. Physiol.* 275: C1660–C1667.
36. Dobretsov, M., and J. R. Stimers. 1997. Na/K pump current in guinea pig cardiac myocytes and the effect of Na leak. *J. Cardiovasc. Electrophysiol.* 8:758–767.
37. Stengl, M., K. Mubagwa, E. Carmeliet, and W. Flameng. 1998. Phenylephrine-induced stimulation of Na^+/Ca^{2+} exchange in rat ventricular myocytes. *Cardiovasc. Res.* 38:703–710.
38. Tseng, G. N., R. B. Robinson, and B. F. Hoffman. 1987. Passive properties and membrane currents of canine ventricular myocytes. *J. Gen. Physiol.* 90:671–701.
39. Cerbai, E., A. Crucitti, L. Sartiani, P. De Paoli, R. Pino, M. L. Rodriguez, G. Gensini, and A. Mugelli. 2000. Long-term treatment of spontaneously hypertensive rats with losartan and electrophysiological remodeling of cardiac myocytes. *Cardiovasc. Res.* 45:388–396.
40. Ehrlich, J. R., T. J. Cha, L. Zhang, D. Chartier, L. Villeneuve, T. E. Hebert, and S. Nattel. 2004. Characterization of a hyperpolarization-activated time-dependent potassium current in canine cardiomyocytes from pulmonary vein myocardial sleeves and left atrium. *J. Physiol.* 557:583–597.
41. Yao, J. A., M. Jiang, J. S. Fan, Y. Y. Zhou, and G. N. Tseng. 1999. Heterogeneous changes in K currents in rat ventricles three days after myocardial infarction. *Cardiovasc. Res.* 44:132–145.
42. Luo, C. H., and Y. Rudy. 1991. A model of the ventricular cardiac action potential. Depolarization, repolarization, and their interaction. *Circ. Res.* 68:1501–1526.
43. Luo, C. H., and Y. Rudy. 1994. A dynamic model of the cardiac ventricular action potential. II. Afterdepolarizations, triggered activity, and potentiation. *Circ. Res.* 74:1097–1113.
44. Puglisi, J. L., and D. M. Bers. 2001. LabHEART: an interactive computer model of rabbit ventricular myocyte ion channels and Ca transport. *Am. J. Physiol.* 281:C2049–C2060.
45. Ramirez, R. J., S. Nattel, and M. Courtemanche. 2000. Mathematical analysis of canine atrial action potentials: rate, regional factors, and electrical remodeling. *Am. J. Physiol.* 279:H1767–H1785.